






Single-molecule dynamics of Dishevelled at the plasma membrane and Wnt pathway activation

Wenzhe Ma^{a,1}, Maorong Chen^{b,1} , Hong Kang (康宏)^a , Zachary Steinhart^c, Stephane Angers^{c,d}, Xi He^{b,2}, and Marc W. Kirschner^{a,2} 

^aDepartment of Systems Biology, Harvard Medical School, Boston, MA 02115; ^bF. M. Kirby Neurobiology Center, Children's Hospital Boston, Harvard Medical School, Boston, MA 02115; ^cDepartment of Pharmaceutical Sciences, Leslie Dan Faculty of Pharmacy, University of Toronto, Toronto, Ontario, M5S 3M2, Canada; and ^dDepartment of Biochemistry, University of Toronto, Toronto, Ontario, M5S 3M2, Canada

Contributed by Marc W. Kirschner, May 26, 2020 (sent for review June 20, 2019; reviewed by Taekjip Ha, Roeland Nusse, and Jean-Paul Vincent)

Dvl (Dishevelled) is one of several essential nonenzymatic components of the Wnt signaling pathway. In most current models, Dvl forms complexes with Wnt ligand receptors, Fzd and LRP5/6 at the plasma membrane, which then recruits the destruction complex, eventually leading to inactivation of β -catenin degradation. Although this model is widespread, direct evidence for the individual steps is lacking. In this study, we tagged mEGFP to C terminus of *dishevelled2* gene using CRISPR/Cas9-induced homologous recombination and observed its dynamics directly at the single-molecule level with total internal reflection fluorescence (TIRF) microscopy. We focused on two questions: 1) What is the native size and what are the dynamic features of membrane-bound Dvl complexes during Wnt pathway activation? 2) What controls the behavior of these complexes? We found that membrane-bound Dvl2 is predominantly monomer in the absence of Wnt (observed mean size 1.1). Wnt3a stimulation leads to an increase in the total concentration of membrane-bound Dvl2 from $0.12/\mu\text{m}^2$ to $0.54/\mu\text{m}^2$. Wnt3a also leads to increased oligomerization which raises the weighted mean size of Dvl2 complexes to 1.5, with 56.1% of Dvl still as monomers. The driving force for Dvl2 oligomerization is the increased concentration of membrane Dvl2 caused by increased affinity of Dvl2 for Fzd, which is independent of LRP5/6. The oligomerized Dvl2 complexes have increased dwell time, $2 \sim 3$ min, compared to less than 1 s for monomeric Dvl2. These properties make Dvl a unique scaffold, dynamically changing its state of assembly and stability at the membrane in response to Wnt ligands.

Wnt signaling pathway | Dishevelled | single molecule | protein complex size | fluorescence

The Wnt pathway is a central and conserved developmental pathway in all metazoans. Some of the genes of this pathway originated in choanozoans but the core pathway is clearly already established in sponges, tens of millions of years before the Cambrian explosion. Examples of the conserved role of the Wnt pathway include: anterior-posterior axis formation in embryos, in organogenesis, and in tissue homeostasis (1–3). Dysregulation of the Wnt pathway plays a role in various human diseases, including skeletal, cardiac vascular diseases (4), and cancer (5). Animals generally have multiple Wnt ligands, e.g., 19 Wnt ligands and 10 Fzd, 1 LRP5, and 1 LRP6 receptor proteins in mammals. In the off state of the canonical Wnt pathway, β -catenin levels are low, due to active proteolysis mediated by a conserved set of proteins associated in a putative destruction complex (6). The destruction complex might very well be structurally flexible, with no well-defined stoichiometry. In the absence of a Wnt signal, the scaffold proteins APC and Axin bind β -catenin and recruit the kinases CK1 α and GSK3. A priming phosphorylation on β -catenin mediated by CK1 α leads to further phosphorylation by GSK3. The phosphorylated β -catenin is then recognized and ubiquitinated by the E3 ligase β -TrCP, and then targeted by the proteasome for degradation. Wnt ligand binding to the Fzd and LRP5/6 receptors at the plasma membrane somehow interferes with this process and therefore causes a buildup of β -catenin protein (the rate of protein

synthesis is unaffected by Wnt pathway activation) (7). The Wnt signal for inhibiting degradation is thought to proceed by interference with the activity of CK1 α and GSK3. Several molecular mechanisms for the Wnt-mediated repression of GSK3 activity have been proposed. These models include ones where Wnt-induced LRP5/6 phosphorylation acts as a pseudo substrate and directly inhibits GSK3 activity (8), or Wnt-induced Axin1 dephosphorylation and a conformational change leads to dissociation of β -catenin and Axin1 (9), or Wnt-induced receptor endocytosis drives GSK3 into multivesicular bodies, sparing the cytosolic β -catenin from phosphorylation (10).

Apart from APC and Axin, a third scaffold protein, Dvl (Dishevelled) plays an essential but cryptic role in Wnt pathway activation. It must be critical, as its loss completely abolishes the activation of the pathway and leads to constitutive β -catenin degradation regardless of Wnt addition (11). But the means by which Dvl carries out its essential function are still not defined. Unlike APC and Axin, which primarily work as scaffolds allowing for the assembly of the putative destruction complex, Dvl's only apparent role in the canonical Wnt pathway is inhibiting the destruction complex. One popular model is that Dvl bridges the destruction complex and the receptors, communicating the effect

Significance

Canonical Wnt signaling is one of the most important and widely distributed pathways in metazoan development. Dishevelled is thought to serve as an essential bridge between the membrane receptors and downstream signaling components, which has the tendency to aggregate in vitro and to form large aggregates of dubious significance in vivo, when overexpressed. To obtain a molecular understanding of the role of Dvl in Wnt signaling, while circumventing these aggregation problems, we have expressed a fluorescent-tagged Dishevelled in cells at its physiological concentration and quantified the size distribution of Dishevelled before and after Wnt treatment. We found that limited oligomerization in response to the Wnt ligand is very dynamic and provides a key step in signal transduction.

Author contributions: W.M., M.C., X.H., and M.W.K. designed research; W.M., M.C., and H.K. performed research; Z.S. and S.A. contributed new reagents/analytic tools; W.M. and M.C. analyzed data; W.M. and M.W.K. wrote the paper; and W.M. built mathematical models.

Reviewers: T.H., Johns Hopkins University; R.N., Stanford University School of Medicine; and J.-P.V., The Francis Crick Institute.

The authors declare no competing interest.

This open access article is distributed under [Creative Commons Attribution-NonCommercial-NoDerivatives License 4.0 \(CC BY-NC-ND\)](https://creativecommons.org/licenses/by-nc-nd/4.0/).

¹W.M. and M.C. contributed equally to this work.

²To whom correspondence may be addressed. Email: xi.he@childrens.harvard.edu or marc@hms.harvard.edu.

This article contains supporting information online at <https://www.pnas.org/lookup/suppl/doi:10.1073/pnas.1910547117/-DCSupplemental>.

First published June 29, 2020.

of Wnt binding perhaps by interacting with both Fzd and Axin1. In this view, Dvl performs its task by binding to the intracellular region of Fzd and forms a receptor complex together with the coreceptor LRP5/6 in what is known as the signalosome (12). Dvl may remain as a stable complex or shuffle on and off the membrane (8, 13). Dvl may also guide Axin1 and other components to the plasma membrane which may then disrupt the destruction complex and repress its β -catenin degradation activity. Much of the evidence supporting this model has come from biochemical and imaging experiments with overexpressed Wnt pathway components. While approaches based on protein overexpression can be informative, they have potential limitations, if concentration is important to the properties of the system. This state of uncertainty ultimately can only be clarified by direct visualization of dynamics of pathway components at their physiological levels.

In studies of pathway dynamics, the importance of expressing proteins in cells at their physiological levels cannot be over-emphasized. Overexpression, which is widely used, comes with caveats of potential artifacts. The Wnt pathway scaffold proteins have dimerization (14, 15) or oligomerization (16, 17) domains that carry with them the potential for forming large and potentially nonphysiological structures when expressed at very high concentrations (18–20). Whether these structures ever exist in the physiological context remains a matter of debate. Specifically, the DIX domain of Dvl exhibits linear head-to-tail oligomerization, and overexpressed Dvl forms so-called “puncta” (17, 21–24), which are protein structures as big as $1 \sim 2 \mu\text{m}$ in some cases (over a million Dvl molecules if composed only of Dvl). A physiological function for these puncta of Dvl has been proposed by some groups as scaffolds to repress the destruction complex (17, 21) and challenged by others (25). With the help of modern CRISPR approaches for endogenous tagging of proteins, we are now able to ask questions of the form of Dvl when expressed at a physiological concentration. With total intensity reflection fluorescence (TIRF) microscopy, it is possible to measure dynamic processes at the subsecond time scale with a spatial resolution that allows the resolution of individual molecular-sized complexes. Using such approaches, we have addressed anew the size and dynamic features of membrane-bound Dvl complexes during Wnt pathway activation and analyzed the control of Dvl binding at the plasma membrane.

Results

Most Dvl2 Is Evenly Distributed in the Cytosol Regardless of Exposure to Wnt3a. To measure the distribution of Dvl, we fused mEGFP to the C terminus of the *dishevelled2* gene in HEK293T cells

using CRISPR/Cas9-mediated genome editing. HEK293T cells express all three Dvl genes; Dvl2 represents more than 80% of the total pool (26). Indeed deletion of Dvl2 results in the most severe phenotype among the Dvl gene deletions in mouse models (27). In knockin (KI) HEK293T cells, the concentration of Dvl2-mEGFP varies within 8% of the concentration of the Dvl2 in wild-type (WT) cells; judging from the intensity of Western bands, the response of β -catenin kinetics to Wnt3a is nearly identical to the WT control (Fig. 1A). All of the experiments are done in the presence of 100 nM LGK974 to decrease the autocrine Wnt signal activation. When we imaged Dvl2-mEGFP knockin cells for 10 h by confocal microscopy after the cells were activated by Wnt3a, Dvl2-mEGFP was evenly distributed in the cytosol and rarely found in the nucleus or on the membrane (Fig. 1B and Movie S1). In a few cells, some Dvl2 is localized to a structure that might correspond to the centrosome (28) or endosomes (29). The lack of any discernible plasma membrane localization is likely to be due to the high background of cytosolic Dvl2. Indeed, when we overexpressed SNAP-tagged Fzd5 in the same cells (SI Appendix, Fig. S1), we found some Dvl2 proteins clearly colocalized with SNAP-Fzd5 at the plasma membrane. Presumably the number of Dvl2 complexes on the membrane before or after Wnt3a treatment is very low, either due to low density of membrane Fzd or weak interaction between Dvl and Fzd.

TIRF Visualization and Quantification of Dvl2 Oligomer States on the Plasma Membrane before and after Wnt Addition. To overcome the limitations of confocal microscopy, we imaged the labeled Dvl2-KI cells using TIRF microscopy. TIRF microscopy illuminates to a depth of about 150 nm above the coverglass, which greatly reduces the fluorescence glow from the deeper cytosol. A total of 100 nM LGK974 was added the day before the imaging experiment to decrease the autocrine Wnt signaling. Dvl2-KI cells were imaged once every 30 s for 75 min, with exposure time of 100 ms; Wnt3a (200 ng/mL) was added to the cell culture media at 15 min and images were processed with u-Track (30) (an example of single-molecule detection shown in SI Appendix, Fig. S2). There is a question of whether the cell is accessible to the Wnt3a proteins at its lower surface facing the coverglass. To test this, we measured the diffusion of a cell-impermeable organic dye (CLIP-Surface 647) together with recombinant Wnt3a protein randomly labeled with the Alexa 555 dye. By imaging at the TIRF plane, we found that the cell bottom surface is accessible to both organic dye and labeled Wnt3a. We also found that the Wnt3a appears at similar time underneath or surrounding the cell, indicating fast accessibility

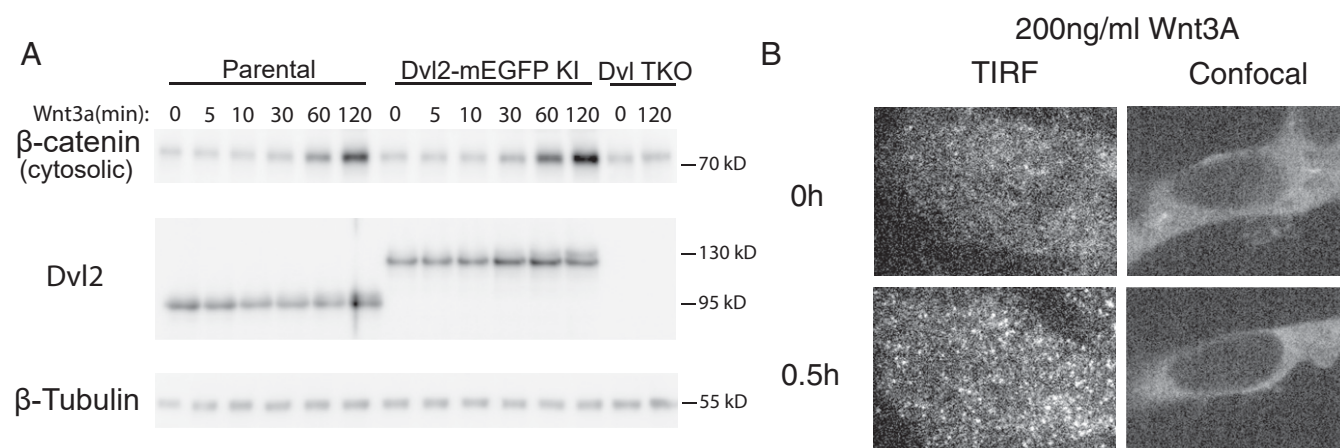


Fig. 1. Dvl2 forms complexes on the cell membrane in response to Wnt3a treatment. (A) β -Catenin concentration increases while Dvl2 concentration remains constant within 2 h after Wnt3a treatment, both in HEK293T cells and Dvl2-mEGFP knockin cells. β -Catenin shows no change in Dvl-TKO cells after Wnt3a treatment. (B) Confocal images of Dvl2-mEGFP show no clear change after Wnt treatment while TIRF images show clear membrane localization.

of the cell bottom surface to the ligands, with most of the delay coming from the diffusion in the bulk media instead of underneath the cell (*SI Appendix, Fig. S3*).

To determine the number of Dvl2-mEGFP in each complex, we used two methods to quantitate single mEGFP intensity. We first analyzed the intensity distribution of all of the fluorescent spots in one image; second, we analyzed the precipitous jumps of intensity of the spots in temporal traces. We assumed that these jumps were either due to photobleaching or to association/dissociation of Dvl2-mEGFP subunits. The absolute value of all of the signals (Fig. 2C) or intensity jumps in the spots (Fig. 2B and D) were compiled into histograms and fitted with a Gaussian mixture function to establish the single mEGFP intensity value. The ratio of mean mEGFP intensity achieved from the two methods is 1.09 ± 0.16 (six control datasets). The first method does not require high-quality long single-molecule traces, so we have generally used it in later analyses to quantify the mEGFP intensity. As another measurement of single-molecule fluorophore intensity, we measured a tagged membrane protein mEGFP-GlyR α 1, which yielded a similar single mEGFP intensity value (*SI Appendix, Fig. S4*).

One important factor affecting the quantification of complex size is the maturation of mEGFP. In previous studies, it is estimated that about 50% (31) to 80% (32) of the mEGFP are bright by estimating the visible subunit in the tetrameric receptor GluK2. Similarly, we quantified the percentage of bright mEGFP in live HEK293T cells by fitting the size distribution of mEGFP-GluK2 tetramers. We concluded that the size distribution is best explained by a maturation ratio of 75% (*SI Appendix, Fig. S5*). Both the total number and oligomer size of Dvl2 complexes will be affected by the invisible Dvl2-mEGFP molecules. We corrected the total number or density by dividing 0.75, and corrected the size distribution by solving a set of linear equations described in *SI Appendix, Supplementary Text S1*. From this point forward we only make use of the corrected number.

In the absence of Wnt, we observed that $85.2 \pm 3.8\%$ of membrane Dvl2 complexes contain only a single Dvl2, with $14.8 \pm 3.8\%$ containing two molecules of Dvl2, virtually none of the spots had more than two Dvl2 molecules. Within 5 min of Wnt3a treatment, there was an increase in the number of Dvl2 molecules localized to the cell membrane which reaches a maximum at 15 min, gradually declining to a level that was higher than before Wnt3a treatment (Fig. 2E and *Movie S2*). This time scale ($t_{1/2}$) of membrane Dvl increase is very similar to the decrease of fully (T41/S37/S33) phosphorylated β -catenin, well before there is a measurable increase in β -catenin concentration (30 min), as observed in bulk assays (7). Following Wnt treatment, monomeric Dvl2 was still the majority of the population, comprising $56.1 \pm 2.2\%$ of the total complexes, although there was a significant shift to larger complexes. By 15 min, $28.4 \pm 2.4\%$ of the complexes contained two Dvl molecules and the rest (15.5%) more than two. As a result, the weighted average size of Dvl oligomers increased from 1.1 to 1.5 (Fig. 2F).

To estimate the number of Dvl2 bound to the plasma membrane, we first estimated the cellular Dvl2 concentration in a single HEK293T cell, to be 140 nM (*SI Appendix, Fig. S6*). With a cell volume of 1.94 pL (measured by ORFLO), on average there should be a total of 1.6×10^5 molecules of Dvl2 per cell. We estimated the bottom area of the cells by quantifying images (*SI Appendix, Fig. S7*) which allows us to estimate the area density of Dvl2 to be $\sim 0.54/\mu\text{m}^2$ (Fig. 3B) after Wnt3A treatment. Assuming the cell to be spherical, its total surface area would be about $7.5 \times 10^2 \mu\text{m}^2$ (note that a model of a flattened cell as an oblate ellipsoid of revolution with an axial ratio of 4 and the same volume of the cell would have a surface area about twice as large, $1.6 \times 10^3 \mu\text{m}^2$). On the membrane, therefore, there should be between 4.1×10^2 molecules of Dvl for a spherical cell model and 8.6×10^2 molecules of Dvl for the oblate ellipsoid of a

revolution cell model. In either case there would be less than 0.6% of the cellular Dvl2 on the membrane, even at peak Dvl2 recruitment. This small fraction of Dvl at the membrane together with high cytosolic Dvl2 background helps explain why membrane Dvl was invisible by confocal microscopy and why it could only be detected by TIRF microscopy.

A Mass Action Description of Dvl-Fzd Interactions after Wnt Treatment. The change in oligomerization of Dvl on the membrane in response to Wnt3a is likely due to homotypic interactions between Dvl molecules and heterotypic interactions between Dvl and Fzd. Since TIRF microscopy can quantitatively measure the size and distribution of Dvl membrane complexes, we have tried to explain the Dvl changes with the simplest possible mass action model. We consider only Fzd and Dvl, where Fzd is the membrane receptor that binds Dvl. Dvl alone can form linear head-to-tail oligomers mediated through its DIX domain (17). Thus, there are two basic binding reactions in the model, Dvl-Dvl binding and Dvl-Fzd binding. We define the dissociation constant between Dvl molecules to be K_D , and the heterotypic dissociation constant between Dvl and Fzd to be K_F . Once on the membrane, we expect that proteins might have different binding affinities due to changed local concentration and membrane-induced constraints on protein structure, such as an effective lower dielectric constant (33). We assume all Dvl complexes that contain Fzd are on the membrane. As explained in *SI Appendix, Supplementary Text S2*, we converted Fzd membrane density to equivalent three-dimensional (3D) concentration, to simplify the calculation. We correct for the membrane effects on both association constants by adding a factor α (<1) to indicate the increased binding affinity of Dvl with other molecules once bound to Fzd. We then have the following mass action equilibrium equations:

$$d_{n-j,m} + d_{j,0} \xrightleftharpoons{K_D} d_{n,m} \quad (n-j \geq m \geq 0)$$

$$d_{n,0} + \text{Fzd} \xrightleftharpoons{K_F} d_{n,1}$$

$$d_{n-j,m-k} + d_{j,k} \xrightleftharpoons{\alpha K_D} d_{n,m}$$

$$d_{n,m-1} + \text{Fzd} \xrightleftharpoons{\alpha K_D} d_{n,m} \quad (n \geq m \geq 1).$$

Here $d_{n,m}$ represents the concentration of one specific configuration of Dvl complexes that contains n Dvl molecules and m Fzd molecules. Note that $d_{n,0}$ contains 0 Fzd, thus representing cytosolic Dvl complexes. The first equation describes Dvl complex formation in the cytosol, or the binding of cytosolic Dvl complexes to the membrane Dvl complexes through Dvl-Dvl interaction. The second equation shows the recruitment of cytosolic Dvl complexes to the membrane by Fzd. The third equation describes the combining and splitting of membrane-bound Dvl complexes, and the fourth equation denotes the binding and unbinding of membrane-bound Dvl complexes to Fzd. α in the last two equations represents general membrane effects. At equilibrium, we can solve for the concentration of all forms of Dvl complexes. Note that there are only five parameters in the model, and we can fix Dvl concentration with our experimental measurements. This allows us to explore the behavior of the model in the full parameter space.

The increased localization of Dvl to the membrane during Wnt pathway activation could be explained by an increase in Dvl protein concentration, or an increase in its binding affinity. When we measured the concentration of Dvl by Western blot in response to Wnt, there was $<20\%$ change in the 4-h period after Wnt treatment (Fig. 1A and *SI Appendix, Fig. S8*). During this time there was a 30 ~ 40% decrease of Fzd during the first hour

of Wnt activation (as measured by the level of overexpressed surface mEGFP-Fzd1 with TIRF microscopy, *SI Appendix, Fig. S9*). Given little change in total cellular Dvl and no increase in Fzd concentration, the remaining possible explanation for increased Dvl at the membrane must be due to a decrease of either K_D or K_F or both. To explore the model further we fixed α , Dvl_0 , and Fzd_0 and asked how changes in K_D and K_F affect the amount of Dvl at the membrane.

The parameter α changes the apparent concentration on the membrane and in turn determines the degree by which the membrane environment affects both Dvl-Dvl binding and Dvl-Fzd binding. We tried $\alpha = 0.5 \sim 0.001$ and found that α does not

affect the general shape of the membrane Dvl size distribution. For further analysis of the oligomerization of Dvl, we chose an arbitrary value for α , which we fixed at 0.01. The Dvl concentration, as measured experimentally, is 140 nM. As stated in *SI Appendix, Supplementary Text S2*, we converted Fzd membrane density to an equivalent 3D concentration to simplify the calculation. We do this by multiplying the ratio of the cell surface area to the membrane density of Fzd and then divide by the cell volume, or just divide the molar number of Fzd to cell volume; 1,200 Fzd molecules per cell is equivalent to 1 nM. We assumed the Fzd concentration to be 10 nM in our calculation; higher or lower concentrations do not qualitatively change the following

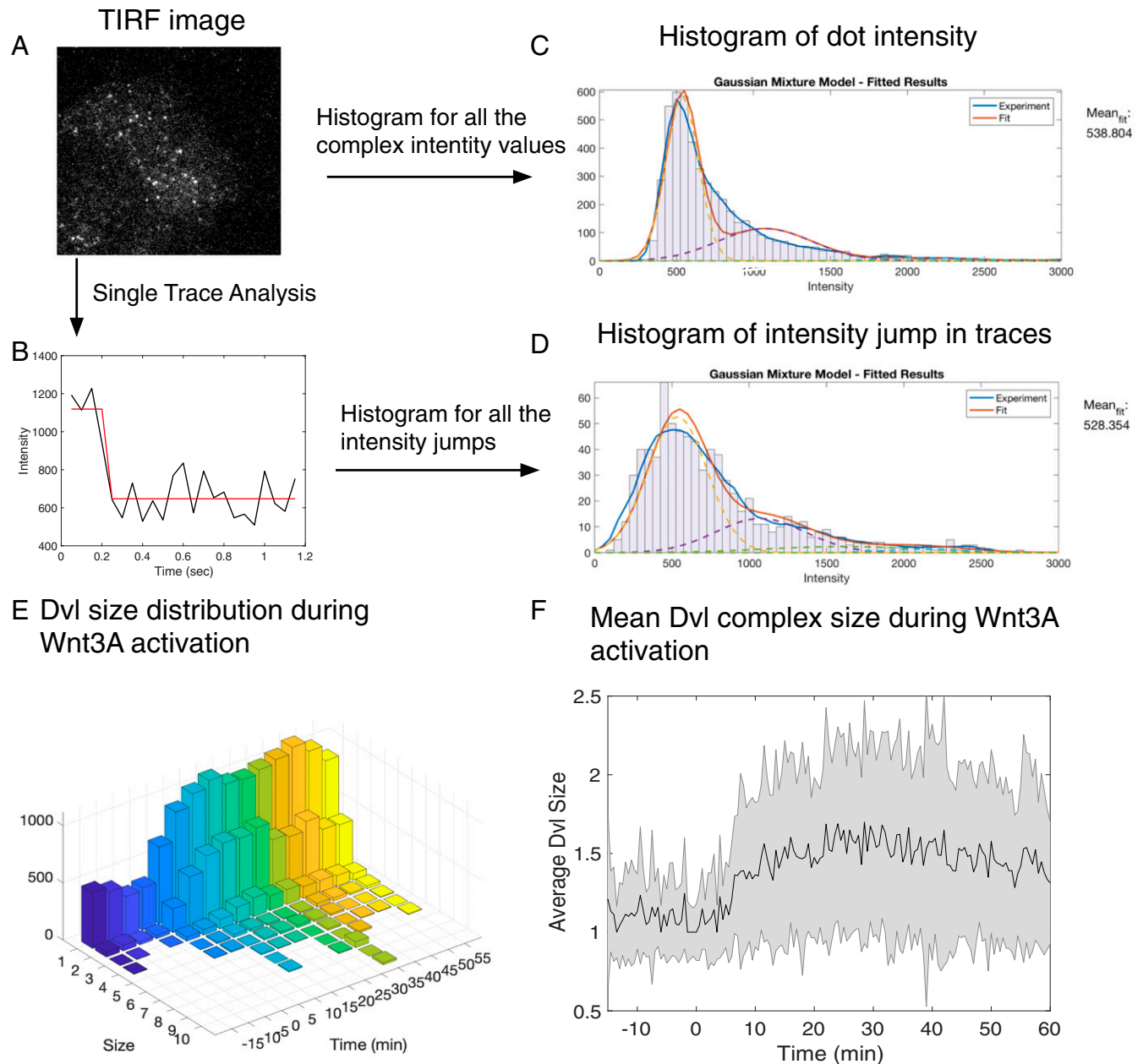


Fig. 2. Quantification of the size and dynamics of membrane Dvl during Wnt pathway activation. TIRF images (A) are analyzed and single-molecule traces (B) are extracted using u-Track. The traces are then used to identify steps where mEGFP intensity increases or decreases. Either the fitted intensity of all of the spots in one image (C) or all of the steps of the single-molecule traces (D) are analyzed to extract single mEGFP intensity value. (E) The time course of Dvl2-mEGFP size distribution is then quantified with the corresponding single mEGFP intensity value. In the experiment, 200 ng/mL Wnt3a was added at $t = 0$ min. (F) Weighted mean size of Dvl2-mEGFP complexes increases from 1.1 to 1.5.

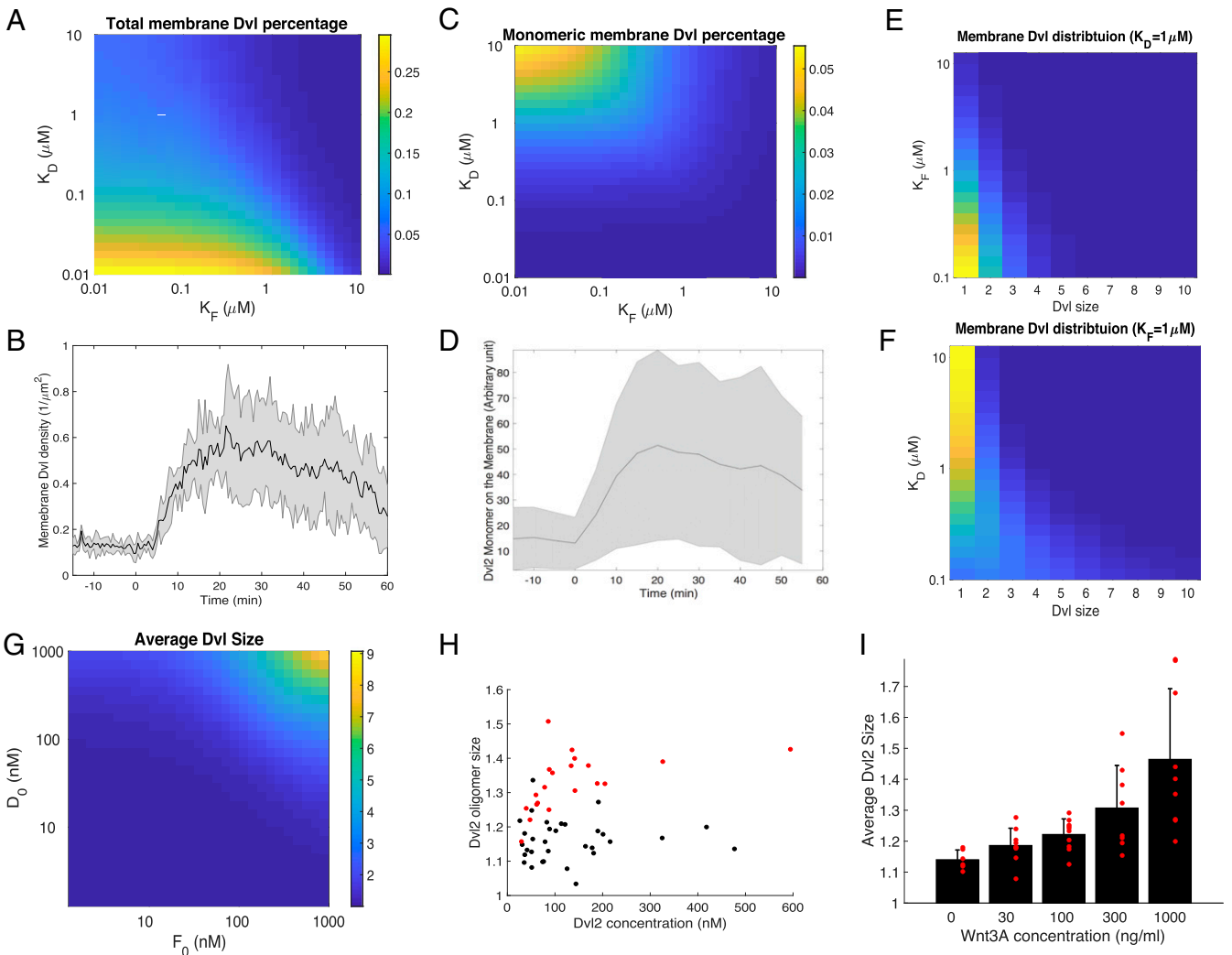
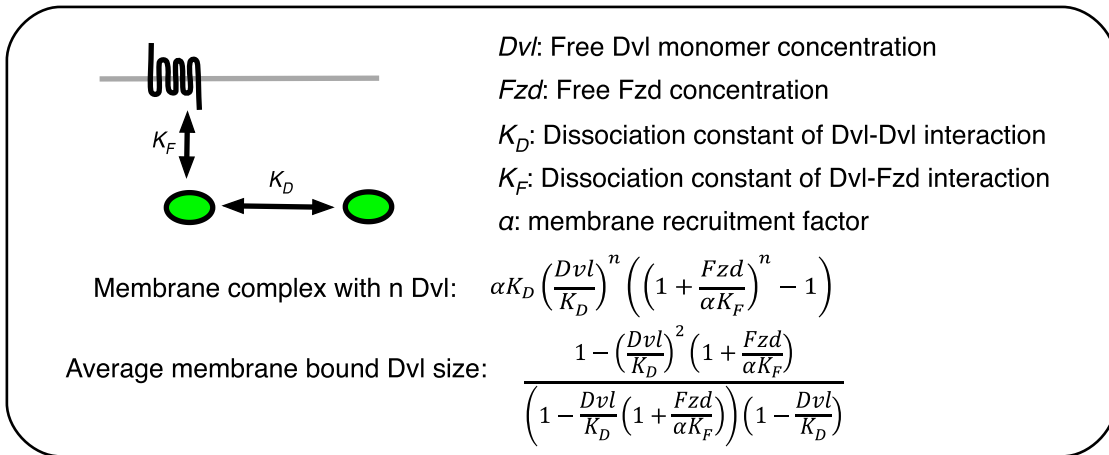


Fig. 3. Dvl membrane recruitment is driven by increased Dvl-Fzd interaction. (A) Predicted percentage of membrane-bound Dvl while varying K_D and K_F . (B) Experimental measurement of total membrane-bound Dvl2 molecules during Wnt3a treatment. (C) Predicted monomeric Dvl on the plasma membrane when varying K_D and K_F . (D) Experimental measurement of membrane-bound monomeric Dvl2 during Wnt3a treatment. (E) Predicted Dvl size distribution with K_D fixed while varying K_F . (F) Predicted Dvl size distribution with K_F fixed while varying K_D . (G) Predicted average size of Dvl complexes while varying Dvl and Fzd concentration. (H) Average size of Dvl complexes while changing total Dvl2 concentration. Each dot corresponds to a single cell. Black dots are cells without Wnt3a treatment while red dots are cells with Wnt3a treatment. (I) Average size of Dvl complexes while varying Wnt3a concentration.

conclusions. Not surprisingly the model predicts that a decrease (increase the binding affinity) of either K_D or K_F can result in increased membrane-bound Dvl (Fig. 3A), as we observed in our experiments (Fig. 3B). However, by computing the average Dvl complex size from the model (*SI Appendix, Fig. S10*), we find that the average size increases to more than 2 when K_D is in the sub μM range, indicating weak Dvl-Dvl interactions in the cell. This is in the same range as found in previous studies ($5 \sim 15 \mu\text{M}$ in ref. 17 and $5 \mu\text{M}$ in ref. 34). Furthermore, we found that to explain the large increase in monomeric membrane Dvl there must be a decrease (increased binding affinity) in K_F but not in K_D (Fig. 3 C and D). This systematic search of parameter space strongly suggests that Wnt treatment acts primarily by increasing the binding affinity between Fzd and Dvl (a decrease in K_F). It is worth noticing that Fzd may undergo dimerization or oligomerization in the presence of Wnt ligands. How would that affect the predictions of the model? Unfortunately, the analytical formulas needed to calculate the effect of dimerization are too complicated for us to derive. Instead, we show with a simple example that Fzd dimer helps to recruit Dvl complexes to the plasma membrane through avidity effect (*SI Appendix, Supplementary Text S3*). Indeed, we don't know the molecular mechanism of the increased Fzd-Dvl binding affinity. Both a change in protein configuration or receptor dimerization/oligomerization are candidate mechanisms.

The size distribution of Dvl contains rich information about molecular interactions. We find that K_D controls the shape of the distribution while K_F controls the height of the distribution (*SI Appendix, Fig. S11*). Decreased K_D favors large Dvl oligomers which flattens the distribution, while increased K_D skews the distribution to monomeric Dvl. On the other hand, a decreased K_F would increase Dvl-Fzd binding which in turn increases the total membrane-bound Dvl, resulting in the distribution shifting upward, while a larger K_F would move the distribution downward. By comparing the experimental distributions (Fig. 2E) to theoretical ones (Fig. 3 E and F), we conclude that the shift-up of the experimental distribution after Wnt3a treatment must be due primarily to decreased K_F (stronger Dvl-Fzd binding). A more complete set of simulations covering a larger parameter range can be found in *SI Appendix, Fig. S11*. Based on the ratio of membrane Dvl to total Dvl, and the shape of the distribution, we estimate that in the absence of Wnt, both K_D and K_F are weak, in the micromolar range.

The model also predicts that an increased concentration of either Dvl or Fzd should result in an increased average Dvl oligomer size (Fig. 3G). Presumably an increase in Dvl concentration will increase the oligomerization of Dvl through its DIX domain, thereby increasing the oligomerization of Dvl in the whole cell, including the membrane. An increased Fzd concentration, on the other hand, increases the membrane local density of Dvl which will be the driving force for larger oligomers. Both predictions can be verified experimentally. To vary Dvl concentration in the cell, we overexpressed Dvl2-mEGFP in Dvl-TKO cells, which had all three Dvls knocked out (KO) (11), and measured cytosolic concentrations with wide-field fluorescence microscopy and Dvl2 size on the membrane with TIRF microscopy. We found a weak but positive correlation between increased Dvl2 size and an increased Dvl2 total concentration. Dvl2 size further increases in response to Wnt3a (Fig. 3H). We use an indirect way to change the apparent Fzd concentration, by adding different concentrations of Wnt. As predicted by the model, Wnt3a should induce a population of Fzd with higher binding affinity to Dvl. Indeed, increased Wnt3a concentration produces a higher average Dvl oligomer size on the plasma membrane (Fig. 3I).

Structural Requirements for Dvl Plasma Membrane Recruitment. In principle Dvl could be recruited either by direct interactions with Fzd or through intermediate proteins. Dvl is known to have three

globular domains: DIX, PDZ, and DEP. It has been shown recently that the DIX and DEP domains in Dvl are important for canonical Wnt pathway function (11). To test which domains affect the membrane dynamics of Dvl, we individually removed the DIX, PDZ, or DEP domains from the Dvl2-mEGFP construct and assayed the effects on Wnt activation, using a transcriptional TOPFlash assay (Fig. 4A and B). When we overexpressed $\Delta\text{DEP-Dvl2}$ in Dvl-TKO cells, it failed to rescue the Wnt pathway activity. The ΔDIX mutant showed a very low degree of complementation. Notably expression of $\Delta\text{PDZ-Dvl2}$ strongly complemented the knockout, but not to the original level. There were corresponding effects of expressing these constructs on Dvl recruitment (Fig. 4F). In TIRF measurements for the above cell lines, we found that cells expressing $\Delta\text{DEP-Dvl2}$ failed to recruit additional Dvl to the membrane after Wnt3a addition and the Dvl on the membrane did not increase its degree of oligomerization. We also found the membrane density of $\Delta\text{DEP-Dvl2}$ to be lower than WT-Dvl2. By contrast the $\Delta\text{DIX-Dvl2}$ complemented the membrane Dvl density to a similar level as WT-Dvl2 but did not show increased level of Dvl binding or oligomerization upon Wnt addition. Dvl deleted in the PDZ domain behaves very similarly to WT-Dvl both in the level of binding and the increased membrane localization and oligomerization in response to Wnt (Fig. 4 E and F). These properties of the Dvl2 mutants attest to the importance of Dvl membrane recruitment in Wnt pathway activation and the central importance of the DIX and DEP domains.

Similar experiments allowed us to test whether the membrane recruitment of Dvl depends on Fzd or LRP5/6. We made Dvl2-mEGFP knockin cell lines in a Fzd-null (all Fzd knockout) cell line, and similarly in an LRP-DKO (LRP5/6 double knockout) (35) cell line. In cells lacking Fzd, we found no Dvl membrane recruitment upon Wnt treatment (Fig. 4F), in agreement with the prediction that Fzd-Dvl interaction increases after Wnt treatment. By contrast in LRP5/6 double knockout cells, Dvl2 still increases its localization to the plasma membrane after Wnt treatment, although it fails to activate downstream genes (Fig. 4). Furthermore, while the canonical Wnt pathway inhibitor, DKK1 blocks Wnt induced β -catenin accumulation through direct binding to the Wnt3a binding region of LRP5/6, cells still show increased Dvl2 membrane localization and oligomerization (*SI Appendix, Fig. S12*). Taken together, these experiments show that Dvl membrane recruitment is Fzd dependent but LRP5/6 independent, as previously shown by Jiang et al. with antibody to quantify protein level of pan-Fzd or Lrp6 (36). Dvl is known to be a general mediator of both canonical and noncanonical pathways. Therefore, it is reasonable to expect that the Dvl response is dependent on Fzd but not on coreceptors, such as LRP5/6 or ROR1/2 (37).

The Potential Significance of the Dwell Time of Dvl2 on the Membrane.

Although steady-state descriptions are useful, many complex processes are governed principally by dynamical processes. This is especially true if such processes involve chemical reactions, such as phosphorylation or ubiquitination, where accumulation of the modified form of the protein is driven by the time an individual molecule remains on a site rather than the average occupancy of that site (38). For this reason, we extended our study of the steady-state distribution of Dvl on the membrane to examine the dwell time of individual Dvl complexes. To analyze the dwell time of individual membrane-bound Dvl2 oligomers, we made 20 Hz videos with TIRF microscopy and tracked the protein complexes. These video images show the diffusional movement of the molecule in the plane of the membrane. The persistence of the signal on a given protein is registered by the number of frames that contains a specific protein complex, thus providing the measure of the dwell time. One important complication with Dvl is that in addition to its dissociation from the membrane, photobleaching can also terminate the signal. This is especially true when images

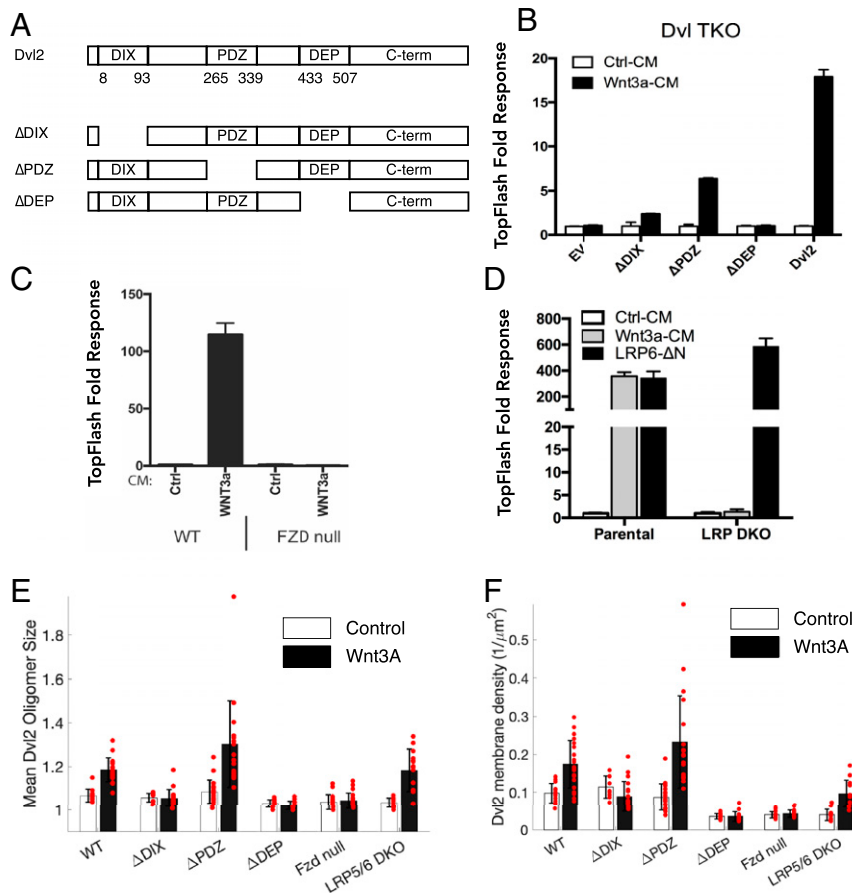


Fig. 4. Dependence of Dvl membrane localization to the Dvl protein domains and receptors. (A) Dvl2 mutations used in the analysis. (B) TOPFlash responses of different Dvl2 mutants (EV, empty vector). (C) TOPFlash responses of Fzd-null cells. (D) TOPFlash assay of LRP5/6 DKO cells. (E) Mean Dvl2 complex size under different conditions. Each dot represents a cell. The error bars represent SD. (F) Dvl2 membrane density under different conditions. The error bars represent SD.

are taken at high imaging rate with a high intensity laser. To correct for the effects of photobleaching, we used a membrane-bound pentameric channel protein GlyR α 1-mEGFP to estimate the rate of photobleaching (*SI Appendix*, Fig. S13); the probability distribution of photobleaching can be approximated as geometric distribution. By this means we estimated the photobleaching first order rate constant to be $1.17 \pm 0.13/\text{s}$, which corresponds to mean half-life of 0.59 s (11.8 frames) for mEGFP.

Two potential reactions could affect the dwell time of Dvl complexes. Dissociation from the membrane will terminate the recording of Dvl complexes in the series of video frames, thus shortening the trace length. On the other hand, the merging of a membrane-bound Dvl with another membrane-bound Dvl or with a new Dvl molecule from the cytosol would extend the trace length (Fig. 5A). Based on these basic processes, we can show by simulation that the dwell time distribution of photobleaching can be modeled by a geometric distribution which decays exponentially with increased dwell time. The distribution would still be geometric after adding the dissociation term, but the experimental traces would have considerably shortened dwell times. When we add merging and splitting of Dvl molecules to the model, it lengthens the apparent dwell time for two reasons: First, merging Dvl complexes introduces fresh fluorophores to the membrane complexes, which counteracts photobleaching; second, the resulting larger complexes have a reduced rate of dissociation (Fig. 5B).

With this framework, we can begin to estimate the dissociation rate for all of the mutants and Fzd KO, LRP5/6 DKO cells. The pooled dwell time distributions of different mutants are shown in Fig. 5C. Wnt3a clearly shifts the distribution to form a long tail for WT-Dvl2, Dvl2- Δ PDZ in Dvl-TKO cells, and in LRP5/6 DKO cells, indicating active Dvl-Dvl association and dissociation events, consistent with the requirement of the DIX domain for Dvl-Dvl interaction and the DEP domain for Dvl-Fzd interaction. We used the steep decline region of the dwell time distribution to approximate the dissociation rate constant (*SI Appendix*, *Supplementary Text S4*), which is shown in Fig. 5D. The fitted dissociation rate constants are in the range of 2 ~ 10/s. The frame rate of the TIRF microscope (20/s) unfortunately limits the precision of our estimate of the dissociation rate constants for these very fast dissociation events. Nevertheless, if we assume an association rate constant of $5 \times 10^5/\text{M}\cdot\text{s}$ for proteins the size of Dvl (39), the dissociation constant will be in the range of 4 ~ 20 μM , which is very weak at a cellular Dvl2 concentration of 140 nM. This estimate of the dissociation constant confirms our estimate based on the modeling of Dvl-Fzd association. Such weak binding explains the small number of Dvl on the plasma membrane (less than 0.3% of the cytosolic concentration) despite relatively high Dvl concentration in cytosol. In the presence of Wnt3a, the average dissociation rate constant for WT-Dvl2 changes from 6/s to 4/s, indicating increased interaction between Dvl and the membrane, presumably through Fzd. This further confirms our analysis of the Dvl size distribution and membrane localization. The

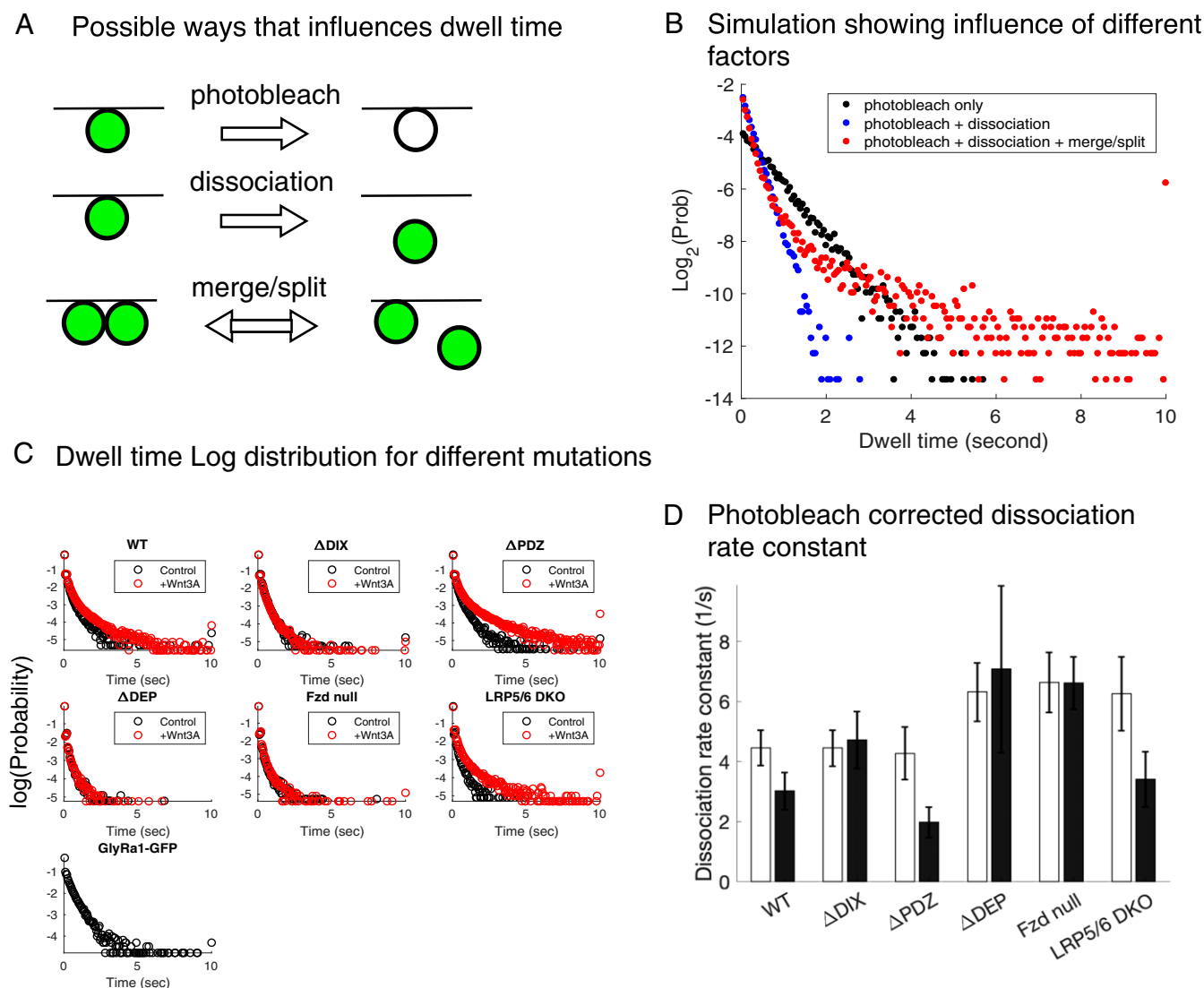


Fig. 5. Dwell time analysis of membrane-bound Dvl. (A) Possible mechanisms that changes the single-molecule dwell time measurement. (B) Simulations to show how different mechanisms affecting dwell time distribution. (C) Pooled dwell time logarithm distribution of different mutant cell lines. (D) Dissociation rate constants derived from the fast time scale of dwell time distribution. The error bars show SD.

change of dissociation rate constant is less than twofold because the number reflects the pairwise interaction change between Dvl and Fzd for a mixed population of Fzd, both Wnt bound and Wnt free. As expected, we found Dvl without the DEP domain increases the dissociation rate from $\sim 6/s$ to $\sim 10/s$, as does Dvl2 in Fzd KO cells, indicating decreased Dvl membrane binding. These mutants also show no change in the dissociation rate constant with Wnt3a treatment. Surprisingly LRP5/6 knockout cells show decreased Dvl membrane binding but still respond to Wnt3a. This suggests that in the absence of LRP5/6 the Wnt3a interaction with Fzd is strong enough to affect the binding affinity of Fzd with Dvl. Dvl- Δ DIX mutants show similar basal membrane binding with wild-type Dvl but do not respond to Wnt3a.

Due to photobleaching, the dissociation rate estimate when averaged in Fig. 5D reflects the time scale of the population with the shortest dwell time. To estimate the dwell time of the relatively few large Dvl complexes that bind more stably to the membrane, we measured their fluorescence recovery after photobleaching. We imaged the recovery process by using 5-s time intervals for 10 min after photobleaching, where the fast time scale $\sim 5/s$ would not show up. This experiment showed that the

recovery time is indistinguishable before (125 ± 65 s) and after (156 ± 96 s) Wnt3a treatment. Arguably this population of large stable complexes would be stable before and after Wnt addition. The dwell time, however, becomes much more than an academic interest, when we consider relevant chemical reactions that might occur at similar time scale.

Dvl is well known to be phosphorylated at multiple sites (40), probably at the plasma membrane, although the exact function of these modifications is unclear. Based on the BRENDA database, which catalogs enzyme kinetic information, the turnover number of general Ser/Thr kinase like CK1 is only $0.057 \sim 0.19/s$, much slower than the fast time scale of Dvl-Fzd interaction ($4 \sim 6/s$) discussed above, but faster than the slow time scale which corresponds to the average Dvl oligomer binding ($0.0083 \sim 0.0056/s$). If Dvl phosphorylation occurs on the membrane in the absence of Wnt, the transient binding (rapid first order dissociation rate) and the low level of Dvl on the membrane would mean that there would be a very low probability that a given Dvl molecule would be phosphorylated during its very short residence on the membrane. Furthermore, phosphatases in the cell will work continuously to remove the existing phosphate group,

lowering the background phosphorylation level. After Wnt pathway activation Dvl oligomers form on the membrane, substantially increasing the dwell time from less than a second to a few minutes and this could allow appreciable phosphorylation. A process dependent on dwell time rather than occupancy would ensure a very low background of Dvl phosphorylation in the absence of Wnt. While the difference of dwell time may seem modest after Wnt treatment, it is arguably sufficient to switch a significant fraction of Dvl complexes from an unphosphorylated state to a phosphorylated state.

If this hypothesis is correct, we would expect phosphorylation to occur with overexpressed Fzd. It would also occur with the PDZ domain-deleted Dvl, but not with DEP domain deletions. We further tested the hypothesis by overexpressing Fzd5 in a Fzd-NUL cell line at increasing Fzd plasmid concentration. We found that Dvl2 phosphorylation increases with Fzd (*SI Appendix, Fig. S14*). Because Fzd recruits Dvl onto the plasma membrane, more Fzd results in higher levels of Dvl and leads to increased phosphorylation. Like WT-Dvl, Δ DIX, and Δ DEP Dvl deletions also show increased phosphorylation (*SI Appendix, Fig. S15*).

How Oligomerization Affects Dvl Dynamics and Thus Activates the Wnt Response. The oligomerization of Dvl complexes appears to be a necessary feature of canonical Wnt pathway activation. Can we say something about whether association of Dvl subunits is itself sufficient to activate the pathway? To answer this question, we generated a series of artificial Dvl oligomers by replacing the DIX domain of Dvl2 with a set of artificially designed helical

bundles, designed to generate specific oligomer states (41). The set of Dvl oligomeric constructs are named dimer, trimer, tetramer, and hexamer which correspondingly contain two, three, four, and six Dvl molecules in stable complexes (Fig. 6A). The size of the various stable oligomeric constructs was confirmed by sucrose gradient sedimentation (*SI Appendix, Fig. S16*). Each of these modified forms of Dvl was separately expressed in Dvl-TKO cells and the activation of the Wnt pathway was measured by the TOPFlash assay. Wnt pathway activation peaks at the Dvl trimer and drops as the Dvl2 size increases further (Fig. 6B). That there is an optimum in the size of the complexes, taken literally means that activity of the native Dvl depends on the proper balance of efficient binding and efficient release.

If the dynamic oligomerization of Dvl2 was important for its function, we should be able to replace the DIX domain with other domains with a similar property of reversible oligomerization and retain Dvl2 protein function. To test this proposition, we used the SAM (Sterile Alpha Motif) domains of the LEAFY transcription factor found in flowering plants. Like the Dvl DIX Domain, SAM has a tendency to form an equilibrium distribution of linear head-to-tail oligomers (42). By replacing the DIX domain of Dvl2 with two different SAM domains (SAM1 from *Arabidopsis thaliana* or SAM2 from *Ginkgo biloba*), we were able to rescue the Wnt pathway activity (Fig. 6C). Point mutations in the SAM domain that disrupt oligomer formation disrupt Wnt pathway activity (SAM1-M, and SAM2-M in Fig. 6C). These experiments strongly suggest that one important function of the DIX domain on Dvl is to form dynamic oligomers.

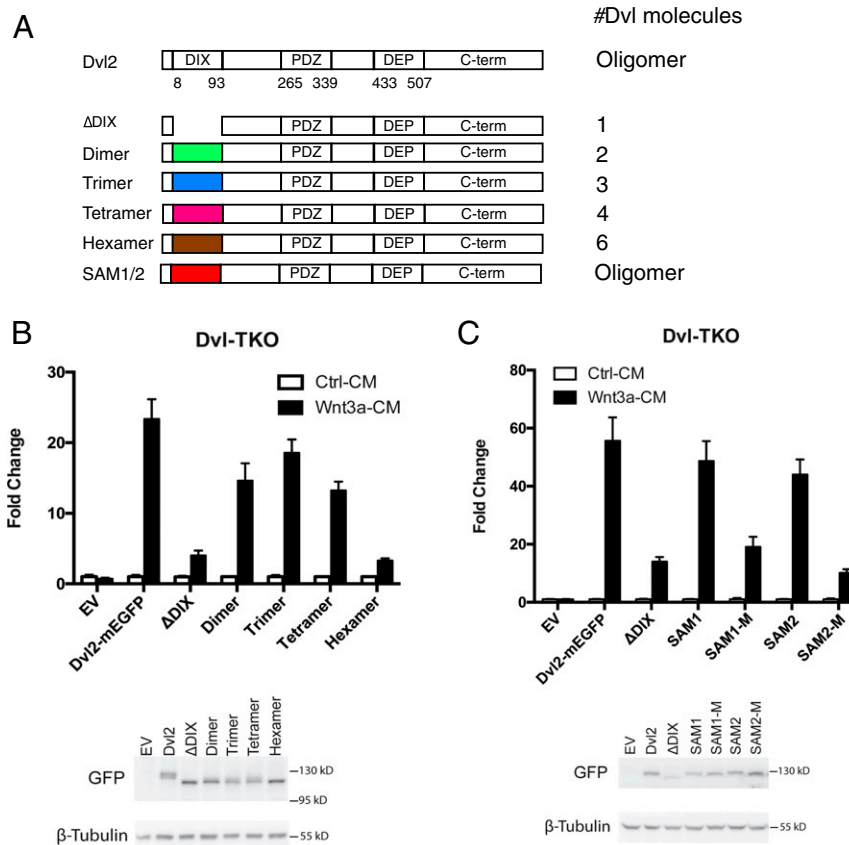


Fig. 6. Both Dvl membrane recruitment and Dvl subunit dynamics are important for Wnt pathway activation. (A) DIX domain of Dvl2 are replaced with artificially designed helical bundles that have specific number of subunits. (B) All of the mutants have lower activity compared to wild-type Dvl2 but the activity peaks at Dvl2 trimer. (C) DIX domain of Dvl2 is replaced with SAM domain from two species of plants. The SAM domains that can oligomerize successfully recover the activity of Wnt pathway, but the SAM domains with monomer mutations could not.

Discussion

Our current mechanistic understanding of the mechanism of Wnt signal transduction focuses around the “destruction complex” and the “signalosome,” concepts which are still speculative. Among the most enigmatic of all of the components of these complexes is the set of essential Dvl scaffold proteins. To assess the function of Dvl in Wnt signaling we have carried out a kinetic study of the behavior of Dvl in living cells, combining CRISPR-induced genome modification with single-molecule imaging, and analyzing the data through quantitative modeling. Our studies of single-molecule imaging coupled with modeling point to a role of Dvl oligomerization at the membrane and the very weak binding between Dvl-Dvl and Dvl-Fzd. These weak and dynamic interactions are very important and for that reason it is important to express labeled proteins in the cell at close to their endogenous levels. We found that Dvl’s interactions in the cell are defined by its relatively high endogenous concentration, which at 140 nM is still significantly lower than DIX domain binding affinity to Fzd in the membrane ($\sim\mu\text{M}$). The disparity between the very low concentration and the weak binding affinity guarantees that the predominant species of Dvl in the cell is in the form of a soluble monomeric pool. The weak binding and rapid off rate allow the Dvl proteins to quickly interrogate various sites in the cytosol and membrane (Fig. 7A). Monomeric Dvl binds to Fzd and dissociates in less than a second. Upon Wnt treatment, increased Fzd-Dvl interaction increases the binding between Fzd and Dvl and in turn increases the local concentration of Dvl (Fig. 7B). The higher local concentration then drives Dvl to form oligomers on the cell membrane. Following Wnt binding the oligomerized Dvl binds at higher stoichiometry, but perhaps most significant feature is that individual Dvl molecules now spend much more time on the membrane, where reactions such as phosphorylation alter the Dvl molecule, which may activate the downstream signaling process (Fig. 7C). Dvl in the larger complexes are still dynamic and come on and off the membrane, with smaller oligomers, more dynamic than larger ones. If these modifications of Dvl are sufficiently stable, they may survive long enough to perturb downstream cytosolic reactions and affect β -catenin turnover.

It should not be surprising that binding affinity to the membrane would in some way determine Dvl activity. It is somewhat more surprising that the effect on downstream processes reaches a maximum activity at the level of a trimer of Dvl and then declines. It is important to note the significant differences between the dynamic oligomers and stable oligomers. WT-Dvl2 forms dynamic oligomers that actively exchange the Dvl subunits in the complexes. Stable oligomers cannot exchange subunits and only associate and dissociate as a whole. In this way, large complexes can be maintained for an extended period of time on the plasma membrane while still remaining inherently dynamic. Small complexes, by contrast come on and off rapidly. The responsiveness of the signal pathway is partially related to the reaction speed of individual reaction steps like phosphorylation. While the reaction speed is hindered by either too strong or too weak binding between the enzyme and the substrate, due to either product inhibition or lack of enzyme-substrate complexes. We assume that Dvl protein complexes are most effective in downstream signaling when they are both stable and dynamic on the membrane, when the binding affinity is neither too strong nor too weak. Nature solves this seemingly incompatible task by designing Dvl protein to be a dynamic scaffold, having one membrane protein binding domain (DEP) and one oligomerization domain (DIX). The DEP domain controls the binding of Dvl to Fzd, while DIX, together with local concentration, controls the size of the Dvl oligomer. The instability of the individual Dvl subunits is related to the relative low binding affinity between DIX domains ($\sim\mu\text{M}$ from our model) (17, 34) and DEP-Fzd ($\sim\mu\text{M}$ from the experiments). When a Dvl complex gets to a certain size, it has multiple DEP

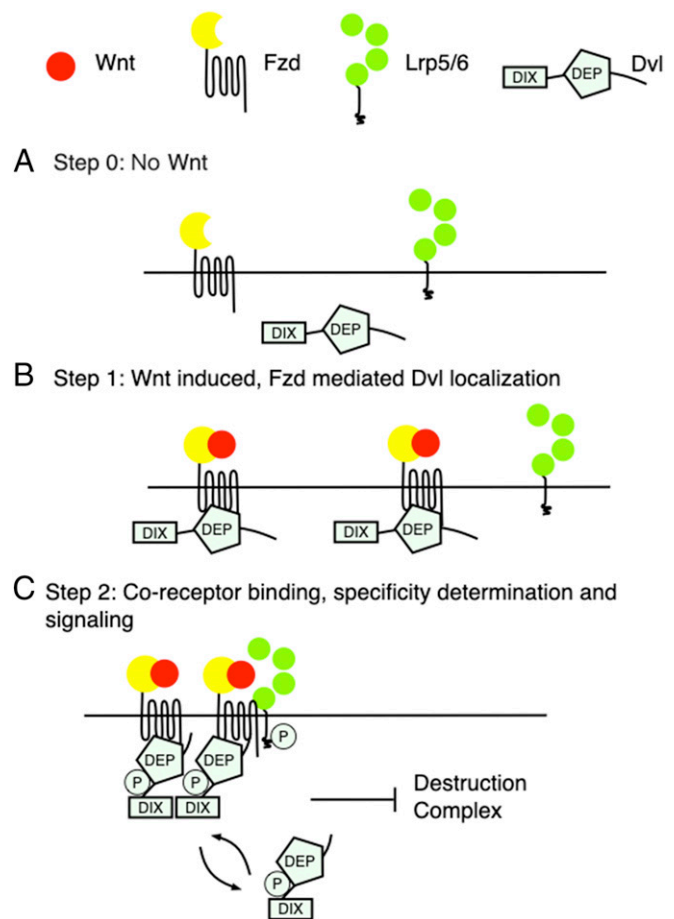


Fig. 7. Summary of Dvl dynamics during Wnt pathway activation. (A) Majority of Dvl are monomers that bind to the membrane transiently. (B) Wnt ligand-induced Dvl membrane localization eventually leads to Dvl oligomerization. (C) Oligomerized Dvl has increased dwell time which enables potential modifications like phosphorylation to happen.

domains that are incorporated into one complex, and this increases the binding to the membrane through an avidity effect.

Dvl oligomers might be confused with puncta in the previous experiments; their nature is very different. The Dvl oligomers in our study (less than five Dvl for more than 90% of the complexes) are far smaller than the puncta in some other studies that could reach the diameter of $1 \sim 2 \mu\text{m}$, potentially containing millions of proteins. The total number of Dvl2 proteins in one cell is only about 160,000 in comparison, so much of the large puncta formation seems to be an artifact of overexpression. We must point out that large complexes involving other Wnt pathway proteins like Axin and APC may in fact form under physiological conditions (20) or that Dvl might form supersized complexes in other biological systems like early embryos (43, 44). It is fair to point out when superphysiological levels of proteins capable of weak dynamic interactions are expressed in cells, the burden of proof on the significance of the structures that are produced lies with the experimenter to show that complexes of similar size and composition actually exist under natural conditions.

We can speculate but do not yet fully understand why Dvl dynamicity is carefully programmed into the system. One explanation may derive from the phosphorylation of Dvl. It is possible that phosphorylation of Dvl is a modulator of Wnt signaling, affecting the dynamicity of Dvl. But a more interesting interpretation is that the dynamicity itself may control the phosphorylation of Dvl and that phosphorylation may in turn control the stability of

β -catenin. The rapid rate of turnover of monomeric Dvl is too fast for modification by typical kinases (although the actual Dvl kinases acting on the Dvl at the membrane could have atypical kinetics). In this view the Wnt signal by stabilizing larger oligomers of Dvl would be required to allow Dvl to persist long enough at the membrane to be phosphorylated. The phosphorylated Dvl might then travel back into the cytosol and inhibit β -catenin degradation. Such a model would be very different from a view that Dvl, and perhaps specifically phosphorylated Dvl, only acts near the plasma membrane to inhibit the “destruction complex.” This is one possible model to explain the activation of the Wnt signaling pathway. To fully understand the process, we will need to work out the detailed mechanism of Dvl phosphorylation and dephosphorylation, including knowledge of the dynamics of kinases and phosphatases in the pathway.

Materials and Methods

Plasmids. Human Dvl2 wild-type cDNA sequence was acquired from Harvard PlasmID (HsCD00326703). The Dvl2 gene is then PCR amplified and moved onto pBABE-puro backbone (Addgene 1764) using Gibson assembly. There is a 12-amino acid linker in between Dvl2 and mEGFP (GGAGGTAGTGGTGGATCTGGTGATCAGGAGTTCT). Dvl2 mutants were made by using Agilent QuickChange II mutagenesis kit (200523) on the basis of the Dvl2-mEGFP plasmid. For the Dvl2 oligomer mutations, all oligomer sequences are from S1 appendix, table S1 of ref. 36. SAM domain sequences are from *A. thaliana* (SAM1) and *G. biloba* (SAM2) (37).

To construct donor vector for Dvl2-mEGFP-knockin, 5' and 3' homology arms (609 bp and 840 bp, respectively) were PCR amplified using genomic DNA of HEK293T as the template and cloned into a vector containing mEGFP.

Cell Culture and Cell Lines. HEK293T and the derived cells were grown at 37 °C and 5% (vol/vol) CO₂ in Dulbecco's Modified Eagle's Medium (DMEM), 10% (vol/vol) fetal bovine serum (FBS), and 1% antibiotics (penicillin/streptomycin).

The Dvl-TKO cell line is the abbreviation of HEK293T cells with all of the Dvl knocked out, which was made by S.A.'s laboratory. Fzd-null is the abbreviation of HEK293T cells with all Fzd knocked out. LRP-DKO is the abbreviation of HEK293T cells with LRP5/6 knocked out. Fzd-Null is the abbreviation of HEK293T cells with all Fzd knocked out, which is a gift from Feng Cong, Novartis, Cambridge, MA. HEK293T cells are from ATCC. The Dvl2-KI cell line is the abbreviation of HEK293T cells with mEGFP knocked in on the C terminus of Dvl2. Dvl2-1Mer are Dvl2- Δ DIX overexpressed in Dvl-TKO cells.

Antibodies and Immunoblotting. Total cell lysates in Nonidet P-40 lysis buffer (50 mM Tris, pH 7.5, 150 mM NaCl, 1 mM EDTA, 1% Nonidet P-40, 10% glycerol, 10 mM NaF, 10 mM Na₂VO₄, and protease inhibitor mixture, pH = 7.4) were prepared by gentle rotating at 4 °C and cleared by centrifugation. Samples were run on an sodium dodecyl sulfate–polyacrylamide gel electrophoresis and transferred to Immobilon-P membrane. A total of 0.015% digitonin in phosphate-buffered saline (PBS) supplemented with 50 mM NaF and protease inhibitor mixture were used to isolate the cytoplasmic fraction of β -catenin. Indirect immunochromatography using a secondary antibody conjugated with horseradish peroxidase was visualized using ECL reagents on an LAS-3000 imager (FujiFilm). The following commercially available antibodies were used: from BD Transduction Laboratories: anti- β -catenin (610154, 1:2,000); from Hybridoma Bank: anti- β -tubulin (E7, 1:5,000); from Cell Signaling Technology, anti-Dvl2 (3216, 1:1,000); from Abcam, anti-GFP (ab13970, 1:1,000); and from R&D Systems, rhWnt-3a (5036-WN).

Dual Luciferase Assay. HEK293T cells (ATCC CRL-11268) were transfected using FuGENE HD (Promega, E2312) in triplicate. Cells were plated in 24-well plates and transfected the following day with 50 ng SuperTOPFlash, 5 ng TK-Renilla. Dual luciferase reporter assays were performed using the Dual-Luciferase Reporter Assay System (Promega, E1960) according to the manufacturer's instructions. Representative results are shown from one of three (or more) independent experiments.

TIRF Experiments. The TIRF experiments were done on a Nikon Ti motorized inverted microscope with Perfect Focus System, 491-nm laser (50 mW max power) with 50-ms exposure time. Images or movies were acquired with MetaMorph software. The microscope has temperature and CO₂ level control to minimize the environment perturbation on cells.

The cells were either grown on γ -irradiated 35-mm glass bottom dishes (MatTek P35G-0.170-14-C) or on high-precision microscope cover glasses (Marienfeld 0117650 lot. 33825 819). The glass was coated with 10 μ g/mL fibronectin (Sigma-Aldrich F0895) in PBS for 10 min before cells were plated. A total of 100 nM LGK974 (Caymanchem 14072) was added to the cell culture medium when the cells were plated to decrease the autocrine Wnt signaling. The cells were cultured in normal DMEM and switched into FluoroBrite (Thermo Fisher A1896701) with 10% FBS and 100 nM LGK974 before imaging. The imaging experiments were normally done the next day after the cells were plated.

Image Analysis of TIRF Experiments. The images from TIRF experiments were analyzed by u-Track (29) from Danuser Lab. The parameters used are 1.3 for point spread function (PSF) sigma, 0.05 for alpha, and 5 for fit window size. The single-molecule intensity distributions and traces were then analyzed with homemade MATLAB codes.

To quantify single mEGFP intensity, we tracked the membrane protein with 20-Hz imaging frequency and then extracted all of the traces longer than 20 steps. These traces were then analyzed with tdetector (45) for step analysis. The step sizes from all of the traces were then fitted with Gaussian mixture model with proportional mean. The peak value of the first Gaussian function was used as the single mEGFP intensity value. The procedure can be applied to either control protein GlyR α 1-mEGFP or Dvl2-mEGFP itself. Another way to estimate the single mEGFP intensity is by fitting the histograms of intensity of all of the complexes in the cell. We compared the two methods and could achieve similar single mEGFP intensity estimations. Step size estimation is more restricted to the quality of single-molecule traces. Transient traces could greatly increase the noise of this method. The intensity histogram method was used in most of the experiments.

All of the plasmids are available on Addgene. Other data, code, and materials will be made available upon request.

ACKNOWLEDGMENTS. We thank the Nikon Imaging Center at Harvard Medical School for providing the imaging environment and for discussing the imaging details. We thank the Imaging and Data Analysis core facility at Harvard Medical School for providing help in analyzing the single-molecule data. We specially thank Feng Cong and Xiaomo Jiang for important contributions to our work. We thank Derek Bowie and Mark Arousseau for providing GlyR α 1-GFP and GluK2-GFP plasmids and for discussing single-molecule quantification methods. We thank Ana R. Hernández, Adrian Salic, Taran Gujral, Ren Sheng, Bryan MacDonald, Kangmin He, and Ying Lu for many helpful discussions. We also thank Mariann Bienz for comments on this work. M.W.K. acknowledges support by National Institute of General Medical Sciences GM26875 and National Institute of Child Health and Human Development HD0731. X.H. acknowledges support by R01GM126120 and R35GM134953, and the Harvard Digestive Disease Center (NIH P30DK034854) and Boston Children's Hospital Intellectual and Developmental Disabilities Research Center (NIH P30HD18655). X.H. is an American Cancer Society Research Professor.

1. A. Wodarz, R. Nusse, Mechanisms of Wnt signaling in development. *Annu. Rev. Cell Dev. Biol.* **14**, 59–88 (1998).
2. T. Grigoryan, P. Wend, A. Klaus, W. Birchmeier, Deciphering the function of canonical Wnt signals in development and disease: Conditional loss- and gain-of-function mutations of β -catenin in mice. *Genes Dev.* **22**, 2308–2341 (2008).
3. D. J. Richter, P. Fozouni, M. B. Eisen, N. King, Gene family innovation, conservation and loss on the animal stem lineage. *eLife* **7**, e34226 (2018).
4. S. Foulquier *et al.*, WNT signaling in cardiac and vascular disease. *Pharmacol. Rev.* **70**, 68–141 (2018).
5. C. Y. Logan, R. Nusse, The Wnt signaling pathway in development and disease. *Annu. Rev. Cell Dev. Biol.* **20**, 781–810 (2004).
6. J. L. Stamos, W. I. Weis, The β -catenin destruction complex. *Cold Spring Harb. Perspect. Biol.* **5**, a007898 (2013).
7. A. R. Hernández, A. M. Klein, M. W. Kirschner, Kinetic responses of β -catenin specify the sites of Wnt control. *Science* **338**, 1337–1340 (2012).

8. B. T. MacDonald, K. Tamai, X. He, Wnt/ β -catenin signaling: Components, mechanisms, and diseases. *Dev. Cell* **17**, 9–26 (2009).
9. S.-E. Kim *et al.*, Wnt stabilization of β -catenin reveals principles for morphogen receptor-scaffold assemblies. *Science* **340**, 867–870 (2013).
10. V. F. Taelman *et al.*, Wnt signaling requires sequestration of glycogen synthase kinase 3 inside multivesicular endosomes. *Cell* **143**, 1136–1148 (2010).
11. M. V. Gammons, T. J. Rutherford, Z. Steinhart, S. Angers, M. Bienz, Essential role of the Dishevelled DEP domain in a Wnt-dependent human-cell-based complementation assay. *J. Cell Sci.* **129**, 3892–3902 (2016).
12. J. Bilić *et al.*, Wnt induces LRP6 signalosomes and promotes dishevelled-dependent LRP6 phosphorylation. *Science* **316**, 1619–1622 (2007).
13. T. Schwarz-Romond, C. Merrifield, B. J. Nichols, M. Bienz, The Wnt signalling effector Dishevelled forms dynamic protein assemblies rather than stable associations with cytoplasmic vesicles. *J. Cell Sci.* **118**, 5269–5277 (2005).
14. G. Joslyn, D. S. Richardson, R. White, T. Alber, Dimer formation by an N-terminal coiled coil in the APC protein. *Proc. Natl. Acad. Sci. U.S.A.* **90**, 11109–11113 (1993).

15. M. Eubelen *et al.*, A molecular mechanism for Wnt ligand-specific signaling. *Science* **361**, eaat1178 (2018).
16. N. Shibata *et al.*, Crystallization and preliminary X-ray crystallographic studies of the axin DIX domain. *Acta Crystallogr. Sect. F Struct. Biol. Cryst. Commun.* **63**, 529–531 (2007).
17. T. Schwarz-Romond *et al.*, The DIX domain of Dishevelled confers Wnt signaling by dynamic polymerization. *Nat. Struct. Mol. Biol.* **14**, 484–492 (2007).
18. T. Sakai, T. Katashima, T. Matsushita, U. Chung, Sol-gel transition behavior near critical concentration and connectivity. *Polym. J.* **48**, 629–634 (2016).
19. P. Li *et al.*, Phase transitions in the assembly of multivalent signalling proteins. *Nature* **483**, 336–340 (2012).
20. K. N. Schaefer, M. Peifer, Wnt/Beta-catenin signaling regulation and a role for bio-molecular condensates. *Dev. Cell* **48**, 429–444 (2019).
21. T. Schwarz-Romond, C. Metcalfe, M. Bienz, Dynamic recruitment of axin by Dishevelled protein assemblies. *J. Cell Sci.* **120**, 2402–2412 (2007).
22. J. D. Axelrod, J. R. Miller, J. M. Shulman, R. T. Moon, N. Perrimon, Differential recruitment of Dishevelled provides signaling specificity in the planar cell polarity and wingless signaling pathways. *Genes Dev.* **12**, 2610–2622 (1998).
23. A. Cliffe, F. Hamada, M. Bienz, A role of Dishevelled in relocating Axin to the plasma membrane during wingless signaling. *Curr. Biol.* **13**, 960–966 (2003).
24. M. Bienz, Signalosome assembly by domains undergoing dynamic head-to-tail polymerization. *Trends Biochem. Sci.* **39**, 487–495 (2014).
25. M. J. Smalley *et al.*, Dishevelled (Dvl-2) activates canonical Wnt signalling in the absence of cytoplasmic puncta. *J. Cell Sci.* **118**, 5279–5289 (2005).
26. Y.-N. Lee, Y. Gao, H. Y. Wang, Differential mediation of the Wnt canonical pathway by mammalian Dishevelleds-1, -2, and -3. *Cell. Signal.* **20**, 443–452 (2008).
27. A. Wynshaw-Boris, Dishevelled: In vivo roles of a multifunctional gene family during development. *Curr. Top. Dev. Biol.* **101**, 213–235 (2012).
28. I. Cervenka *et al.*, Dishevelled is a NEK2 kinase substrate controlling dynamics of centrosomal linker proteins. *Proc. Natl. Acad. Sci. U.S.A.* **113**, 9304–9309 (2016).
29. E. S. Seto, H. J. Bellen, Internalization is required for proper wingless signaling in *Drosophila melanogaster*. *J. Cell Biol.* **173**, 95–106 (2006).
30. K. Jaqaman *et al.*, Robust single-particle tracking in live-cell time-lapse sequences. *Nat. Methods* **5**, 695–702 (2008).
31. H. McGuire, M. R. Arousseau, D. Bowie, R. Blunck, Automating single subunit counting of membrane proteins in mammalian cells. *J. Biol. Chem.* **287**, 35912–35921 (2012).
32. A. Reiner, R. J. Arant, E. Y. Isacoff, Assembly stoichiometry of the GluK2/GluK5 kainate receptor complex. *Cell Rep.* **1**, 234–240 (2012).
33. A. S. Kim, L. T. Kakalis, N. Abdul-Manan, G. A. Liu, M. K. Rosen, Autoinhibition and activation mechanisms of the Wiskott-Aldrich syndrome protein. *Nature* **404**, 151–158 (2000).
34. K. Yamanishi *et al.*, A direct heterotypic interaction between the DIX domains of Dishevelled and Axin mediates signaling to β -catenin. *Sci. Signaling* **12**, eaaw5505 (2019).
35. M. Chen, X. He, APC deficiency leads to β -catenin stabilization and signaling independent of LRP5/6. *Dev. Cell* **49**, 825–826 (2019).
36. X. Jiang, O. Charlat, R. Zamponi, Y. Yang, F. Cong, Dishevelled promotes Wnt receptor degradation through recruitment of ZNRF3/RNF43 E3 ubiquitin ligases. *Mol. Cell* **58**, 522–533 (2015).
37. J. Green, R. Nusse, R. van Amerongen, The role of Ryk and Ror receptor tyrosine kinases in Wnt signal transduction. *Cold Spring Harb. Perspect. Biol.* **6**, a009175 (2014).
38. Y. Lu, W. Wang, M. W. Kirschner, Specificity of the anaphase-promoting complex: A single-molecule study. *Science* **348**, 1248737 (2015).
39. Z.-R. Xie, J. Chen, Y. Wu, Predicting protein-protein association rates using coarse-grained simulation and machine learning. *Sci. Rep.* **7**, 46622 (2017).
40. O. Bernatik *et al.*, Functional analysis of dishevelled-3 phosphorylation identifies distinct mechanisms driven by casein kinase 1 ϵ and frizzled5. *J. Biol. Chem.* **289**, 23520–23533 (2014).
41. S. Brühmann *et al.*, Distinct VASP tetramers synergize in the processive elongation of individual actin filaments from clustered arrays. *Proc. Natl. Acad. Sci. U.S.A.* **114**, E5815–E5824 (2017).
42. C. Sayou *et al.*, A SAM oligomerization domain shapes the genomic binding landscape of the LEAFY transcription factor. *Nat. Commun.* **7**, 11222 (2016).
43. C. J. Peng, A. H. Wikramanayake, Differential regulation of dishevelled in a novel vegetal cortical domain in sea urchin eggs and embryos: Implications for the localized activation of canonical Wnt signaling. *PLoS One* **8**, e80693 (2013).
44. J. R. Miller *et al.*, Establishment of the dorsal-ventral axis in *Xenopus* embryos coincides with the dorsal enrichment of dishevelled that is dependent on cortical rotation. *J. Cell Biol.* **146**, 427–437 (1999).
45. M. Kirschner, J. Gerhart, Evolvability. *Proc. Natl. Acad. Sci. U.S.A.* **95**, 8420–8427 (1998).